Postprint Version

G. McHale, N. J. Shirtcliffe, S. Aqil, C. C. Perry and M. I. Newton, *Topography driven spreading*, Phys. Rev. Lett. 93, Art. No. 036102 (2004); DOI: 10.1103/PhysRevLett.93.036102.

The following article appeared in Physic Review Letters and may be found at http://link.aps.org/doi/10.1103/PhysRevLett.93.036102.

Topography driven spreading

G. McHale*, N. J. Shirtcliffe, S. Aqil, C. C. Perry, M. I. Newton

School of Biomedical & Natural Sciences, Nottingham Trent University

Clifton Lane, Nottingham NG11 8NS, UK

Abstract

Roughening a hydrophobic surface enhances its non-wetting properties into super-hydrophobicity. For liquids other than water, roughness can induce a complete roll-up of a droplet. However, topographic effects can also enhance partial wetting by a given liquid into complete wetting to create super-wetting. In this work, a model system of spreading droplets of a non-volatile liquid on surfaces having lithographically produced pillars is used to show that super-wetting also modifies the dynamics of spreading. The edge speed-dynamic contact angle relation is shown to obey a simple power-law and such power laws are shown to apply to naturally occurring surfaces.

Keywords: Wetting, contact angles, spreading, super-hydrophobic surfaces

PACS Number: 68.08.Bc, 68.03.-g, 68.03.Cd

* To whom correspondence should be addressed. E-mail: glen.mchale@ntu.ac.uk

Liquids and droplets of liquids are of great importance in many processes ranging from ink-jet printing to DNA technologies. Understanding how droplets sit on solid surfaces and how they spread out to form films is relevant to problems as diverse as ring-stain formation due to the drying of spilt drops of coffee[1] to microfluidics[2]. However, solid surfaces are rarely smooth and flat, but are usually rough or have undulations, pores or other surface structure. In recent years, the effect of surface topography on wetting has become the focus of much interest since the demonstration in 1996 by Onda *et al*[3] of a hydrophobic fractal-like surface. Since then, these super-hydrophobic surfaces have been constructed in a wide variety of ways, from lithographic fabrication[4] to transformation of simple plastics[5]. Super-hydrophobic surfaces have a range of interesting properties from droplet impact with a time of contact independent of speed[6] and to drops rolling down these surfaces under capillary forces at a speed faster than a solid sphere would roll under gravity[7]. In nature, some plants, such as *Nelumbo nucifera* (L.) *Druce*, structure the surface of their leaves so that their chemical hydrophobicity is enhanced into super-hydrophobicity[8] and, in the Namibian desert, a beetle, *Stencora sp*., controls the topography of its back surface together with regions of chemical hydrophobicity and hydrophilicity to collect drinking water from fog-laden wind.[9] Super-hydrophobic principles also apply to other liquids whose equilibrium contact angles can also be enhanced by surface roughness or texture. While the topographic enhancement of contact angles to create non-wetting surfaces has been extensively studied, the opposite effect of topography induced reduction in droplet contact angles and increases in the rate of droplet spreading to create super-wetting and super-spreading effects has not been so extensively studied.

For a droplet, hydrophobicity and wetting is governed by the balance of forces at the contact line arising from the three interfacial tensions, γ_{SV}, γ_{SL} and γ_{LV}, occurring at the solid-vapor, solid-liquid and liquid-vapor interfaces, respectively. Projecting the liquid-vapor force horizontally using the contact angle θ and establishing a horizontal force balance gives Young's Law,

$$\cos\theta_e^s = \frac{\gamma_{SV} - \gamma_{SL}}{\gamma_{LV}} \qquad (1)$$

where θ_e^s is the equilibrium contact angle. An alternative view to balancing forces is to consider the interfacial tensions as surface energies per unit area of the interface. In this approach the effect of increasing the area covered by the contact line by a small amount, ΔA,

is to replace the solid-vapor interface by a solid-liquid interface and so change the surface free energy by $(\gamma_{SL}-\gamma_{SV})\Delta A$. In addition, the movement of the liquid creates an additional liquid surface area of $\Delta A\cos\theta$ resulting in a surface free energy increase of $\gamma_{LV}\,\Delta A\cos\theta$.[10] If the surface free energy is to be at a minimum then the overall change in surface free energy must vanish and this gives Young's Law for the equilibrium contact angle (Eq. (1)). Roughness, or topographic structuring, of the surface modifies this argument because the solid surface has a larger area, $r\Delta A$, than the horizontal projection of the area, where r is a roughness factor and is greater than one. Whilst the roughness alters the surface free energy change at the solid interface, it does not alter the liquid-vapor contribution. In energetic terms, the overall effect of topography is to result in an equilibrium contact angle on a rough surface, θ_e^r, given by Wenzel's equation,[11]

$$\cos\theta_e^r = r\cos\theta_e^s \qquad (2)$$

Wenzel's equation predicts that roughness will emphasise the intrinsic wetting behavior of a surface as determined by its surface chemistry. Enhancement of both non-wetting and complete wetting are predicted. If the contact angle on the smooth surface is larger than 90^o, roughness will further increase the observed contact angle, but if it is less than 90^o roughness will reduce the observed contact angle. The changes in hydrophobicity induced by roughness can be large with equilibrium contact angles of ~ 115^o on flat surfaces being converted to angles in excess of 165^o on rough surfaces. Moreover, Wenzel's equation suggests that on a rough surface, complete wetting will be achieved for all partial wetting liquids satisfying $\cos\theta_e^s > 1/r$.

In practice, super-hydrophobic surfaces do not entirely follow Wenzel's equation, but involve incomplete liquid penetration so that the droplet sits on a composite air-solid surface; the contact angle on a smooth surface for which roughness results in non-wetting behavior is then reduced below 90^o.[12] In this form of super-hydrophobicity (or, if the liquid is not water, super-non-wetting) the equilibrium contact angle is determined by the fraction of area of the solid tops, φ_s, in the planar projection of the area rather than the roughness r. The equilibrium contact angle is then given by the Cassie-Baxter equation,[13,14]

$$\cos\theta_e^r = -\varepsilon + \varphi_s\left(\cos\theta_e^s + \varepsilon\right) \qquad (3)$$

where ε=1. In a similar manner, it can be anticipated that the complete wetting predicted by Wenzel's equation will only occur if the surface texture can completely imbibe the volume of the deposited droplet. If it cannot then an equilibrium droplet may form on a composite liquid-solid surface and a Cassie-Baxter type of equation, Eq. (3), but with ε=-1 will likely be valid.[15]

In this work we show that similar considerations leading to modification of equilibrium angles can be applied to the dynamics of liquids spreading on rough or textured surfaces. When a droplet spreads on a smooth and flat surface a Poiseuille flow occurs and a viscous dissipation proportional to $\eta v_E^2/\theta$ is created, where η is the viscosity and v_E is the edge speed of the drop.[10] This dissipation is equal to Fv_E where the driving force F is proportional to the unbalanced component of the liquid-vapor surface tension: $\gamma_{LV}(\cos\theta_e^s - \cos\theta)$. For small angles and complete wetting surfaces (θ_e^s =0^o) this gives the Hoffman-de Gennes Law with the edge speed proportional to the cube of the dynamic contact angle, i.e. $v_E \propto \theta^3$. Roughness will modify the driving force to γ_{LV} ($r\cos\theta_e^s - \cos\theta$) and with the viscous dissipation we predict that for small angles an additional term directly proportional to the dynamic contact angle occurs,[16] i.e.

$$v_E \propto \theta(r-1) + \theta\left(\theta^2 - r\theta_e^{s2}\right)/2 \qquad (4)$$

The derivation leading to this equation ignores any topography induced modification to the logarithmic cut-off term occurring in the viscous dissipation.[10] It is also known that a pre-wetting film can spread ahead of the macroscopic droplet and the thickness of this film, whether the drop effectively spreads on a composite solid-liquid surface and the effect of any slippage have not been included. Nonetheless, eq. (4) provides a first approximation of how dynamic wetting may be modified by surface topography. For complete wetting (θ_e^s=0^o), the effect of roughness is predicted to produce a transition from a cubic law to a linear law[16] and the spreading of the droplet to become determined by the topography. We emphasise here that the topography changes the surface free energies involved in droplet spreading and so the predicted effects are not simply about a film of liquid spreading within the channels defined by the topography.

To test the prediction for topography induced super-wetting we created multiple sets of surfaces structured with circular pillars of diameter 15 μm arranged in a square lattice with a 30 μm lattice parameter across an area of size 1 cm × 1 cm. The heights of the pillars were increased systematically until a maximum height of 70 μm, equal to an aspect ratio greater than four, was achieved; above this height maintaining vertical side walls for the pillars became difficult. These surfaces were fabricated by patterning a layer of SU-8 photoresist (Fig. 1). Equilibrium measurements for drops of water gave contact angles of 84^o on the flat SU-8 and 144^o on the tallest of the patterned surfaces compared to a predicted 146^o from Eq. (3); when hydrophobised these angles were 115^o, 155^o and 155^o, respectively. We therefore conclude that these surfaces demonstrate super-hydrophobic properties of the Cassie-Baxter type (Eq. (3)). We also investigated the wetting and non-wetting properties of these surfaces for a range of liquids by measuring the equilibrium contact angles using small droplets whose volume (~1 μl) could be entirely accommodated within the texture of the surfaces. We observed complete wetting (i.e. film formation) on tall SU-8 pillar surfaces for liquids, such as ethylene glycol, which have contact angles as high as 51^o on the flat SU-8 surface.[17] From this we conclude that a Wenzel type enhancement of complete wetting can occur on these surfaces.

The experiments on dynamic wetting used video-profiles of the spreading of small droplets (initial volume ~ 1 μl) of non-volatile PDMS (polydimethylsiloxane) oils of viscosity 10 000 cSt; PDMS completely wets the flat SU-8 surface. The size of these droplets was less than the capillary length so that surface tension dominates and the shape of the droplet is a spherical cap. From the side-profile images of the drop we determined the volume, contact diameter and dynamic contact angle, and confirmed the validity of the spherical cap shape assumption. The drop volume remained constant over much of the spreading time, but the final stage in the spreading was characterised by the PDMS draining into and filling the surface structure. Visually the separation between the droplet spreading regime and draining into a film

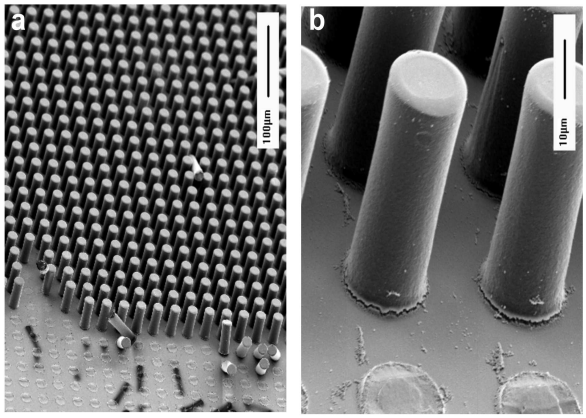

FIG. 1. Scanning electron microscope images of lithographically structured surfaces showing a square lattice of 15 μm diameter cylindrical pillars with a 30 μm lattice parameter: (a) view of a field of pillars, and (b) close-up view of the pillars.

was clear for the surfaces with the tallest patterns. On these patterns the surface structure can be seen in the images, via the surface reflected light, during the period the droplet spreads from initial contact angles of in excess of 70^o down to around $30\text{-}35^o$. As the latter angles occur, the reflected view of the structure of the surface is lost in the image as a film completely fills the pattern at the droplet edge and spreads out in advance of the droplet. During this final stage the drop dynamics changed due to the loss of drop volume and the complication of the drop spreading on a pre-wetting film of the oil. The speed of the droplet spreading for drops of similar volume was visibly faster on the textured surfaces than the flat surfaces. Previous studies of spreading of droplets of PDMS on smooth and abraded glass surfaces have been reported by Cazabat and Cohen[18], but these studies mainly involved data for low contact angles and the film spreading stage. In their work, contact area was measured rather than drop profile. The technique used to produce the abraded surfaces would also have resulted in a constant roughness factor, whereas in our case the roughness factor is varied systematically in a highly controlled manner.

When the volume of a spreading droplet is constant the edge speed can be converted into a rate of change of the angle. For a spherical cap shaped droplet, the edge speed-dynamic contact angle relation for a rough or textured surface becomes,

$$\frac{d\theta}{dt} \propto -\theta^{7/3}\left[(r-1)+\left(\theta^2 - r\theta_e^{s2}\right)/2\right] \qquad (5)$$

For a smooth (r=1) and complete wetting surface (θ_e^s=0^o) this equation integrates to give a simple (Tanner's) power law behaviour, $\theta \propto (t+t_o)^{-n}$ with n=3/10 for the dynamic contact angle.[10,16] If the surface roughness dominates, a simple power law behaviour should still be observed, but with an exponent of n=3/4. In the intermediate regime the exponent n will lie between these two values. Similarly, the edge speed-dynamic contact angle relation (Eq. (4)) will appear to follow a power law $v_E \propto \theta^p$ with the exponents related by $n = 3/(3p+1)$. Equation (5) also predicts that for sufficiently high values of r, liquids which are partially wetting on a smooth surface, but complete wetting on the rough surface, may also follow a power law with n=3/4.

A typical log-log plot of the edge speed (determined numerically from the contact diameter) and dynamic contact angle is shown in Fig. 2; the solid line indicates the initial trend of the slope p. Data equivalent to Fig. 2 where obtained a minimum of six times for each height of pattern and repeated on several separately fabricated surfaces of the same height pattern. Figure 3 shows the log-log plot of the dynamic contact angle data to, corresponding to the data in Fig. 2 and its fit to $\theta = A/(t + t_o)^n$; the percentage change in volume with time is also given and shows that the fit no longer follows the data once the volume loss exceeds ~1 % of the initial drop volume. Analysis of the oscillations in the edge speed indicates that successive maxima and minima correspond to changes in contact diameter of the drop equal to the lattice parameter (i.e. 30 μm); this is due to microscopic stick-slip motion of the droplet edge reflecting the lattice of the pillars.

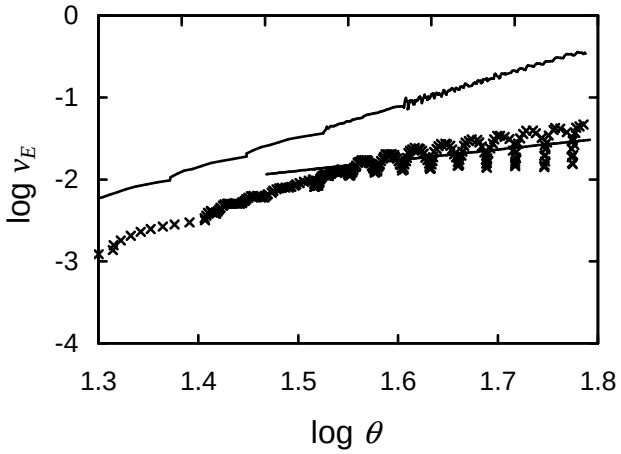

FIG. 2. A log-log plot of the edge speed-dynamic contact angle relationship for a polydimethylsiloxane droplet on a surface with 15 μm diameter pillars of height 45 μm and lattice parameter 30 μm (××× symbols); the slope of this data during the initial spreading (p=1.296) is also shown. The upper solid curve with a slope of p=3 is data for a smooth surface (shifted upwards by 0.5 for clarity).

Figure 4 summarises the complete data set for the spreading exponents of PDMS oils on the multiple surfaces. The data points for the exponent, p, (xxx symbols and left hand axis), show that as the height of the pillars increases in the power-law changes from p=3 towards p=1 as predicted Eq. (4). Exponents p determined using the edge speed-contact angle method are slightly lower than those determined using fits to the dynamic contact angle variation with time, but in both cases the trend from cubic to linear is unambiguous. The dynamic contact angle-time exponent n variation with pillar height ((ooo) indicated by the right-hand

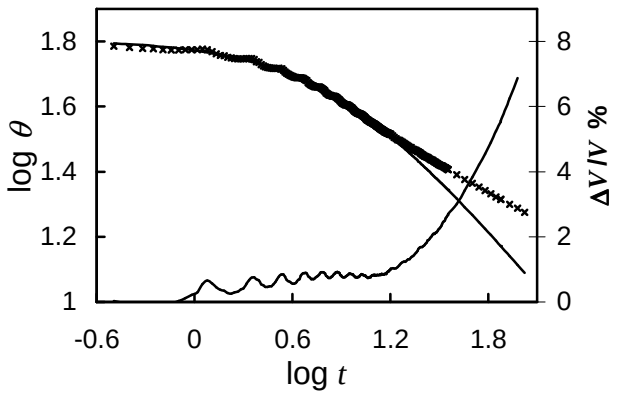

FIG. 3. A log-log plot of the dynamic contact angle and time with a fit of $\theta \propto 1/(t+t_o)^{0.614}$ for the experiment on the textured surface corresponding to the data in Fig. 2. The percentage change in drop volume is also shown (lower curve and right-hand axis).

axis) shows a change from Tanner's Law n=3/10 towards n=3/4 as predicted by Eq. (5). The insets in Fig. 4 show the equilibrium shapes of drops of water on flat and tall patterned surfaces and illustrate that as increasing pattern height causes equilibrium non-wetting of water it can also cause result in faster spreading dynamics for droplets of other liquids. In a final set of experiments, we investigated whether a naturally occurring super-hydrophobic surface would also, when presented with a complete wetting liquid, demonstrate dynamic contact angle behaviour consistent with eq. (4). PDMS oil drops spreading on a sprout leaf (*brassica oleracea*), which has an equilibrium contact angle to water in excess of 165^o, resulted in exponents p~2, thus indicating topography driven spreading.

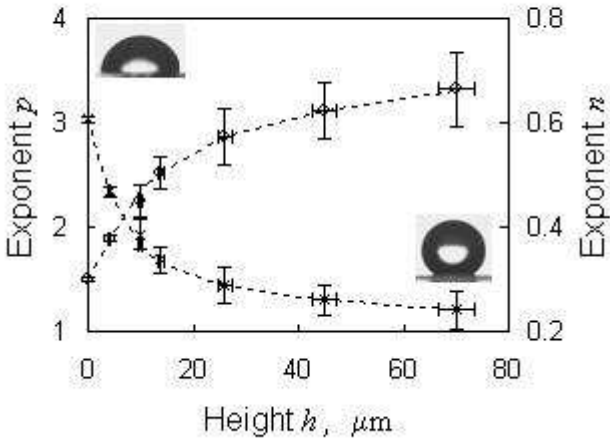

FIG. 4. Exponents p extracted from the edge speed-dynamic contact angle data (×××) for spreading of polydimethylsiloxane oils on textured surfaces; the dotted curve indicates the trend from a cubic to linear form with increasing pillar height. Each data point is an average of experiments on several drops and surfaces. The dynamic contact angle-time exponent n variation with pillar height (ooo) is indicated by the right-hand axis. The inset images show the equilibrium shape of water droplets on the flat surface (θ_e=84^o), and a surface consisting of 52 μm tall pillars (θ_e=142^o).

Our measurements support the idea that a super-hydrophobic surface can also act as a super-wetting surface. Moreover, complete wetting liquids spread on these surfaces at a greater speed than on flat surfaces and their dynamics follow a simple power law behavior. This modification of complete wetting and spreading has significance for processes such as inking, where enhanced spreading is desired, and in coating processes were the maximum coating speed is determined by the dynamic contact angle reaching 180^o. In addition, current attempts to create super-hydrophobic self-cleaning surfaces (e.g. for use in automobile windows) may suffer as a result of the surface roughness/structuring causing difficulty in removing films of oil. Finally, in nature the surface topography used by some plants (and beetles), to achieve water-repellent and self-cleaning surfaces may lead to a greater susceptibility to man-made environmental contamination.

Acknowledgement

The authors' acknowledge the financial support of the UK EPSRC and MOD/Dstl.

References

1. R. D Deegan, O. Bakajin, T. F. Dupont, G. Huber, S. R. Nagel and T. A. Witten, *Nature* **389**, 827 (1997).

2. M. W. J. Prins, W. J. J. Welters and J. W. Weekamp, *Science* **291**, 277 (2001).

3. T. Onda, S. Shibuichi, N. Satoh and K. Tsujii, *Langmuir* **12**, 2125 (1996).

4. D. Öner, T. McCarthy, Ultrahydrophobic surfaces, *Langmuir* **16**, 7777 (2000).

5. H. Y. Erbil, A. L. Demirel, Y. Avci and O. Mert, *Science* **299**, 1377 (2003).

6. D. Richard, C. Clanet and D. Quéré, *Nature* **417**, 811 (2002).

7. D. Richard and D. Quéré, *Europhys. Lett.* **48**, 286 (1999).

8. C. Neinhuis and W. Barthlott, *Annals of Botany* **79**, 667 (1997).

9. A. R. Parker and C. R. Lawrence, *Nature* **414**, 33 (2001).

10. P. G. De Gennes, *Rev. Mod. Phys*. **57**, 827 (1985).

11. R. N. Wenzel, *Ind. Eng. Chem*. **28**, 988 (1936).

12. J. Bico, C. Tordeux and D. Quéré, *Europhys. Lett*. **55**, 214 (2001).

13. R. E. Johnson and R. H. Dettre, in *Contact angle, Wettability and Adhesion*, Advances in Chemistry Series **43**, 112 (1964).

14. D. Quéré, A. Lafuma and J. Bico, *Nanotechnology* **14**, 1109 (2003).

15. D. Quéré, *Physica A* **313**, 32 (2002).

16. G. McHale and M. I. Newton, *Colloids and Surfaces* **A206**, 193 (2002).

17. G. McHale, N. J. Shirtcliffe and M. I. Newton, *Analyst* **129**, 284 (2004).

18. A.M. Cazabat and M.A. Cohen-Stuart, *J. Phys. Chem.* **90**, 5845 (1986).

Figure captions

FIG. 1. Scanning electron microscope images of lithographically structured surfaces showing a square lattice of 15 μm diameter cylindrical pillars with a 30 μm lattice parameter: (a) view of a field of pillars, and (b) close-up view of the pillars.

FIG. 2. A log-log plot of the edge speed-dynamic contact angle relationship for a polydimethylsiloxane droplet on a surface with 15 μm diameter pillars of height 45 μm and lattice parameter 30 μm (××× symbols); the slope of this data during the initial spreading (p=1.296) is also shown. The upper solid curve with a slope of p=3 is data for a smooth surface (shifted upwards by 0.5 for clarity).

FIG. 3. A log-log plot of the dynamic contact angle and time with a fit of $\theta \propto 1/(t+t_o)^{0.614}$ for the experiment on the textured surface corresponding to the data in Fig. 2. The percentage change in drop volume is also shown (lower curve and right-hand axis).

FIG. 4. Exponents p extracted from the edge speed-dynamic contact angle data (×××) for spreading of polydimethylsiloxane oils on textured surfaces; the dotted curve indicates the trend from a cubic to linear form with increasing pillar height. Each data point is an average of experiments on several drops and surfaces. The dynamic contact angle-time exponent n variation with pillar height (ooo) is indicated by the right-hand axis. The inset images show the equilibrium shape of water droplets on a) the flat surface (θ_e=84^o), and b) a surface consisting of 52 μm tall pillars (θ_e=142^o).

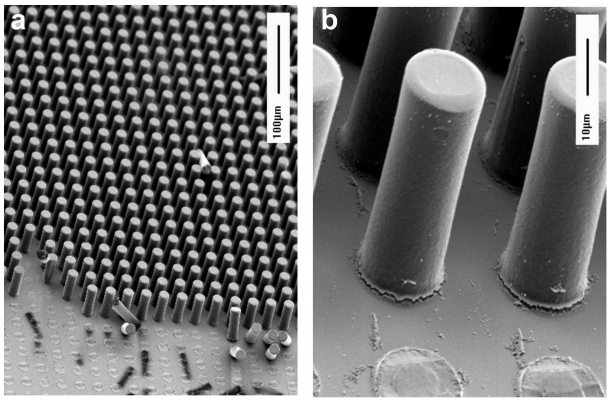

FIG. 1. Scanning electron microscope images of lithographically structured surfaces showing a square lattice of 15 μm diameter cylindrical pillars with a 30 μm lattice parameter: (a) view of a field of pillars, and (b) close-up view of the pillars.

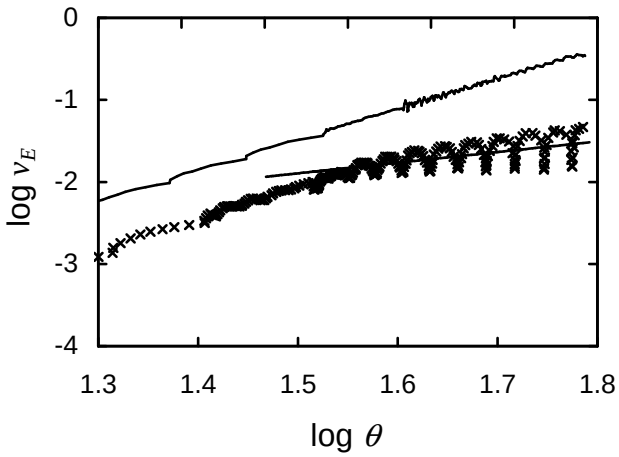

FIG. 2. A log-log plot of the edge speed-dynamic contact angle relationship for a polydimethylsiloxane droplet on a surface with 15 μm diameter pillars of height 45 μm and lattice parameter 30 μm (××× symbols); the slope of this data during the initial spreading (p=1.296) is also shown. The upper solid curve with a slope of p=3 is data for a smooth surface (shifted upwards by 0.5 for clarity).

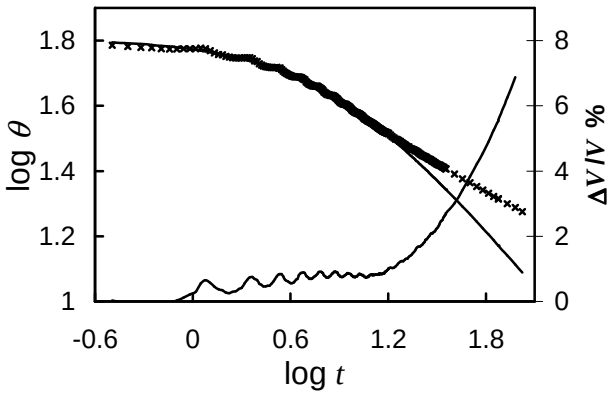

FIG. 3. A log-log plot of the dynamic contact angle and time with a fit of $\theta \propto 1/(t+t_o)^{0.614}$ for the experiment on the textured surface corresponding to the data in Fig. 2. The percentage change in drop volume is also shown (lower curve and right-hand axis).

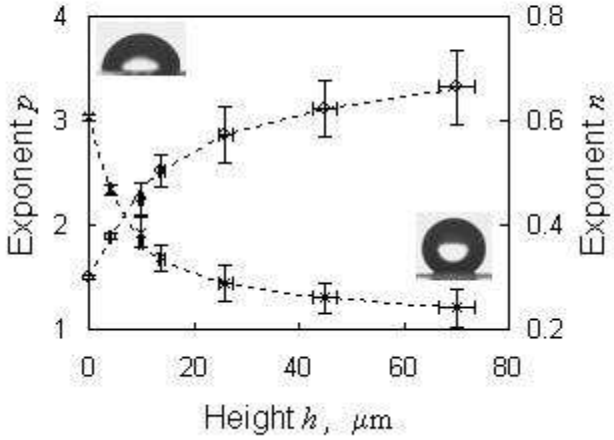

FIG. 4. Exponents p extracted from the edge speed-dynamic contact angle data (×××) for spreading of polydimethylsiloxane oils on textured surfaces; the dotted curve indicates the trend from a cubic to linear form with increasing pillar height. Each data point is an average of experiments on several drops and surfaces. The dynamic contact angle-time exponent n variation with pillar height (ooo) is indicated by the right-hand axis. The inset images show the equilibrium shape of water droplets on the flat surface (θ_e=84^o), and a surface consisting of 52 μm tall pillars (θ_e=142^o).